Flow structures of an electrohydrodynamic two-phase fluid flow in a needle-to-plate negative DC corona discharge

A. Berendt[1], J. Mizeraczyk[2]

[1] *Centre for Plasma and Laser Engineering, The Szewalski Institute of Fluid Flow Machinery, Polish Academy of Sciences, Fiszera 14, 80-231 Gdansk, Poland*

[2] *Department of Marine Electronics, Gdynia Maritime University, Morska 81-87, 81-225 Gdynia, Poland*

Corresponding author: *aberendt@imp.gda.pl*

Abstract This work presents the instantaneous flow images and instantaneous velocity vector fields (obtained by PIV measurements) showing the temporal and spatial evolution of the electrohydrodynamic (EHD) two-phase fluid flow after the negative corona inception in the needle-to-plate electrode arrangement. The measurements were carried out in the initially motionless two-phase fluid (mixture of air and incense smoke particles) closed in the discharge chamber. The corona was supplied by the negative high voltage pulses rising linearly on the needle electrode to a certain value and then staying constant. The results showed that the evolvement of the initially motionless EHD two-phase fluid flow in the closed chamber can be divided into four transient structural stages, i.e. the two-phase free jet stage, the initial stage of two-phase wall-impinging jet, the development stage of two-phase wall-impinging jet and the fully developed two-phase EHD jet, and one final single-phase steady-state stage. The results also confirmed the existence in the two-phase free jet stage the series of the mushroom-like flow structures simultaneously travelling from the needle electrode towards the plate electrode, which has been recorded for the first time in [12].

Keywords: DC corona discharge, EHD, EHD flow, two-phase flow, flow imaging, ESP, PIV

1. Introduction

Motion of electrically charged fluids (gaseous or liquid) in an electric field is the subject of electrohydrodynamics (EHDs). When studying such fluids, it is convenient to distinguish two cases defined by the state of the fluid motion. The first case concerns the fluid being still (motionless) before subjecting it to the electric field. The second one corresponds to the fluid which before applying the electric field is in motion, forming the so-called primary fluid flow. The temporal and spatial structures of both fluids, the motionless and that being in motion change significantly after applying the electric discharge.

Let us limit our consideration to the gaseous fluids, which generally can be single-phase or multi-phase. An example of the single-phase electrically charged gaseous fluid is a single- or multicomponent gas in which a corona discharge has been induced. Air is the typical single-phase multicomponent gas. When the fluid consists of two or more matter phases, it is called a multi-phase fluid. An example of the two-phase fluid is the flue gas in electrostatic precipitators (ESPs), which can be regarded as a mixture of an after-combustion gas (a carrier fluid) and dust (a particulate dielectric matter) suspended in it.

Let us discuss shortly what happens when an electric field is applied to the initially motionless electrically charged single-phase or two-phase fluids (classified by us as the first case regarding the fluid motion). The charging of the fluids can be carried out by another source before applying the electric field, or by the applied electric field itself, for example when after applying the electric field a corona discharge has been induced in the fluid.

In a motionless gaseous single-phase fluid, for example such as air, the forces exerted by the applied electric field on free electron and gaseous ions present in the fluid are transferred during collisions to the neutral molecules through the momentum transfer, setting the latter in motion, i.e. changing the previous motionless status of the fluid. As a result a molecular flow appears, historically called the electric (or recently the ionic) wind (the discovery of the electric wind is credited to Francis Hauksbee (1709), while the name “electric wind” is attributed to Newton [1]). Nowadays, this electrically-induced flow is called an electrohydrodynamic (EHD) molecular flow. The EHD molecular flow redistributes the electric charges in the fluid, which in turn modify the electric field in the fluid. Such a coupling of the electric field, the space charge formed by the electric charges [2-6] and the induced molecular flow causes that the EHD phenomena in the single-phase fluid are complex [7-9].

The EHD phenomena become even more complicated when the fluid consists of two matter phases. An example of such a fluid is an after-combustion gas with dust particulates suspended in it. In the motionless carrier fluid-particulate matter fluid after applying the electric field in the form of corona discharge, first the EHD molecular flow is formed. Then the particulate matter become charged by the gaseous ions and gets subjected to the electric field. Due to it the charged particles form its own EHD flow, which in principle may differ from that of the molecular EHD flow. As a result the EHD interactions include the electric field, the molecular space charge, the dust particle space charge, and two EHD flows: the EHD molecular flow and the EHD particulate matter flow. This makes the EHD flow of such a two-phase fluid very complex.

The above implies that in the initially motionless single- or two-phase fluids closed in chambers of finite volumes a relatively long transient processes occur after applying the electric field (e.g. in the form of corona discharge). After the corona inception in the single-phase fluid, an EHD molecular flow starts to develop into several transient structure forms until the steady-state regime is reached. More complicated situation can be expected after the corona inception in the initially motionless two-phase fluid closed in a finite-volume chamber. The transient phenomena will include the concentration of the particulate matter, the electrical characteristics of the corona, and two EHD flows: the molecular and particulate matter flows formed in the chamber. First, due to the electrostatic precipitation the concentration of the dielectric particulate matter in the chamber will steadily decrease until all particulates deposit on the counter electrode and chamber walls. In this moment the fluid becomes practically single-phase and the single-phase steady-state regime is reached. However, reaching the single-phase steady-state regime takes in total a relatively long time. Second, the corona current, which depends strongly on the concentration of particulate matter [10] will change until the single-phase steady-state regime is reached. Third, after the corona inception the EHD molecular and particulate matter flows will transform through several transition structures into their final form, i.e. the EHD molecular flow will take the final form typical of the single-phase fluid, while the EHD particulate matter flow will cease to exist. So, after the corona inception in the two-phase fluid closed in the finite-volume chamber we will have the continuous transition from the two-phase fluid to the single-fluid, and the single-phase steady-state will be reached after the precipitation of the particulate matter, which takes a relatively long time.

A different situation is when the single-phase or two-phase fluid is in motion (classified by us as the second case with the primary flow). Then an additional factor, i.e. the primary flow has to be considered in the EHD interactions after the corona inception. Now a so- called secondary EHD flow is induced in the continuously oncoming primary fluid flow, and the both flows, the secondary EHD and the primary interacts. If the primary flow is single-phase, the coupling of the electric field, the space charge formed by the electric charges, the secondary EHD molecular flow and the primary flow (also molecular) will take place. This new coupling factor, i.e. the primary flow can significantly modify the EHD phenomena occurring in the continuously oncoming primary flow compared with that initially being motionless. The modification will concern the EHD processes in the transient and steady-state regimes in terms of their structural forms, timings and durations. When the primary flow is two-phase, the image of the EHD phenomena described for the motionless medium case changes as follows. First of all, now we deal with a flowing system, to which the two-phase fluid (a carrier gas-particulate matter) is continuously supplied. Thus, although the particulate matters will be continuously removed from the incoming primary flow by the electrostatic participation, a steady-state balance of the particulates in the system is achievable. As a consequence, in such a steady-state case the corona current will stabilize. This will result in the steady-state structural forms of the EHD molecular and particulate matter flows. Assuming that the precipitation efficiency of the particulate matter is lower than 100%, the transition from the two-phase fluid to the single-phase fluid will not be completed in the system. In the steady-state still we will deal with the two-phase flow, in contrast to the case of the initially motionless two-phase fluid in the finite-volume chamber. Concluding, the transition and steady state structures, their timings and durations for the flowing two-phase fluid should differ from those of the initially motionless two-phase fluid case.

It is worth pointing out that the existence of the transient regime in the EHD flows, in particular in the two-phase fluid flows, in the duration of which the electrical and flow parameters change calls into question the sense of fairy-common measuring the so-called current-voltage characteristics of the corona discharge in the transient regime.

Our preliminary experiments on the temporal and spatial development of EHD particle flow in an initially motionless two-phase fluid (air with suspended incense smoke particles) in the needle-to-plate corona discharge [11], carried out by the imaging and PIV technique, showed clearly the existence of the transient EHD particle flow regime, which has been transforming through several structural stages into the steady-state regime. These transient structural stages were: the two-phase (air-smoke particles) free jet stage (i.e. not interacting with the discharge chamber walls), the initial stage of two-phase wall-impinging jet, the development stage of two-phase wall-impinging jet and the fully developed two-phase EHD jet continuously developing into the single-phase (air) steady-state stage (not reached in the experiment presented in [11]). The flow structure of the two-phase free jet stage of the EHD particle flow recorded in [11] was difficult to explain on the basis of common understanding of the generation of EHD (ionic) wind in the negative corona discharges in electronegative gases (i.e. also in air). After revising our preliminary experiment [11] we concluded that presumably due to the insufficient temporal resolution of recording the EHD particle flow images we have missed some structural details of the two-phase free jet stage. Our recent more accurate repetition of the preliminary experiment presented in [11] has revealed more details of the EHD particle flow in the two-phase free jet stage [12]. The high temporally-resolved recordings of the EHD particle flow images showed the formation of several EHD particle flow substructures simultaneously travelling along the interelectrode gap during the two-phase free jet stage (i.e. in the first stage of the two-phase transient regime).

This paper presents results of an experimental study of the highly-resolved temporal and spatial development of EHD flow in an initially motionless gaseous two-phase fluid subjected to the negative DC needle-to-plate corona discharge. The gaseous two-phase fluid was initially motionless air with smoke particles (incense smoke) homogeneously suspended in it. The two-phase fluid was closed in an acrylic box.

The studies were performed for the negative high voltage pulses rising linearly on the needle electrode to a certain value and then staying constant. This means that both regimes of the EHD two-phase fluid flow, i.e. the transient two-phase flow regime with all its stages and the steady-state single-phase regime could be studied.

The results of investigations include instantaneous flow imaging and instantaneous velocity vector fields measured using 2D Time-Resolved Particle Image Velocimetry (TR PIV) method.

2. Experimental set-up

The experimental apparatus for the study of EHD two-phase fluid flow consisted of an acrylic box with a needle-to-plate electrode arrangement inside, high voltage supply, high-voltage probe, ammeter, digital oscilloscope and 2D TR PIV equipment.

The acrylic box (L:W:H = 600 mm:120 mm: 50 mm), in which the needle-to-plate electrode arrangement was placed, was filled with still air with smoke particles suspended in it (the size distribution of the smoke particles (incense smoke) can be found in [13]). Before each measurement the box was filled with new air having the smoke particle homogeneously distributed in it. The initial concentration of the smoke particles was about 450 000 particles/cm^3.

The needle-to-plate electrode arrangement consisted of two electrodes, a needle and a plate. The needle electrode was made of a stainless-steel rod (1 mm in diameter), the end of which had a tapered profile with the tip having a radius of curvature of 75 µm. The plate electrode was also made of a stainless-steel. The interelectrode gap was 25 mm. The negative high-voltage was applied to the needle electrode through a 3.3 MΩ resistor. The plate electrode was grounded.

The temporally-resolved measurements of the EHD two-phase fluid flow were carried out for a rectangular high voltage pulse rising linearly to a certain value and then remaining constant. The negative voltage pulse was generated by a high-voltage DC power supplier (Spellman High Voltage Electronics Corporation, SL50PN300). The rise rate of pulse front was 13.5 kV/s. The pulse amplitude was - 12 kV (measured between the needle electrode and the plate electrode using the high-voltage probe Tektronix, P6015A). After reaching the constant value by the voltage pulse the average corona discharge current was measured with the ammeter (Brymen, BM859CFa). The average corona discharge changed with decreasing concentration of smoke particles, which have been continuously removed from the chamber volume due to the particle precipitation. It increased from about 15 µA at a particle concentration of 450 000 particles/cm^3 (the first transient flow stages of two-phase fluid) to about 21 µA when only traces of the smoke particles remained in the almost single-phase fluid flow stage (i.e in the “smoke particle-free” air).

The temporally-resolved PIV system was used for both the flow imaging and the instantaneous velocity vector field measurements. It consisted of a twin Nd:YLF laser (Litron, the wavelength of 527 nm, 2 laser pulses (a laser pulse pair) of a power of 30 mJ each), imaging optics (cylindrical telescope), high speed CMOS camera (Phantom, Miro M340, camera sensor size of 2560 pixels × 1600 pixels, acquisition rate of 800 Hz at full frame), digital signal generator (BNC, 575) for triggering the laser pulses and camera shutter, computer for controlling the temporally-resolved PIV system, which recorded the captured images and performed digital analysis of the captured images. The smoke particles, which constituted the particulate matter phase were employed as tracers in the PIV measurements. More detailed description of our temporally-resolved PIV system and measurement procedure can be found in [12].

The timing for the flow imaging and PIV measurements was set as follows: the repetition rate of the laser pulse pairs was set at 300 Hz (i.e. the time between onsets of two consecutive laser pulse pairs was 3.33 ms), the time between two pulses (constituting the laser pulse pair) was set to 170 µs. For the flow imaging the first image of the image pair was used. The instantaneous velocity vector fields were computed using Dantec DynamicStudio software. The spatial resolution of instantaneous velocity vector fields was 0.6 mm × 0.6 mm.

3. Results

The instantaneous images of the evolution of the electrohydrodynamically-induced movement of the suspended particles, shown in this paper are instantaneous maps of the laser light scattered by the suspended smoke particles in the observation plane formed by the laser beam. Higher intensity of the scattered light recorded from a given area of the observation plane corresponds to a higher concentration of the particles present in this area. Dark spots or black areas in the image show areas of little suspended smoke particle concentrations. According to the principles of PIV the velocity vector maps present the velocity fields of the particles moving in/with the carrier gas. However, in some cases, when the particles and carrier gas move together, the recorded velocity vector maps describe also the movement of the carrier gas.

The instantaneous images and instantaneous velocity field maps were recorded for selected times on the voltage pulse rising front and after reaching by the pulse its ultimate amplitude. We found that the EHD two-phase fluid flow began when the rising pulse front reached a voltage of about – 3.9 kV, i.e. 290 ms after the voltage has started to rise. In the following images and maps, the time of EHD particle flow onset is taken as a reference time t = 0.

Typical results of the flow imaging and corresponding instantaneous velocity field maps of the EHD two-phase fluid flow evolution are shown in Fig. 1. The instantaneous flow images for a time period from $t = 2.5$ ms to $t = 80$ ms (Figs. 1 a-i) presents the first stage of the two-phase EHD jet development in the interelectrode gap. At this stage the EHD jet did not interact with the discharge chamber walls, thus we called this stage the two-phase free jet stage.

The image in Fig. 1a ($t = 2.5$ ms) shows the onset of smoke particle removal from the close vicinity of the needle electrode tip. A dark area in the form of a mushroom cap is formed at the needle electrode tip. We will call such a structure a mushroom-like minijet.

The velocity vector map in Fig. 1a shows that in the very first stage of the EHD two-phase fluid flow only the suspended particles presented in the vicinity of needle electrode tip started to move. The starting velocity of the front of the mushroom-like minijet was about 0.1 m/s.

The next image, taken at a time $t = 10$ ms (Fig. 1b) shows that a second mushroom-like minijet has been generated. The first and second mushroom-like minijets were moving downwards. It is worth noticing lighter layers on the mushroom-like minijet fronts. These minijet front layers were formed by the pushed-down smoke particles. The both mushroom minijets were growing when moving downwards. The PIV velocity field in Fig. 1b show that the EHD two-phase fluid flow expanded into the whole area between the needle electrode and the plate electrode. The images in Figs. 1 c–i (the time period from $t = 20$ ms to $t = 80$ ms) show the further development of the EHD two-phase fluid flow and the generation of several new mushroom-like minijets in the first stage of the EHD two-phase flow development. The flow velocity in the jet core increased from about 0.1 m/s at a time $t = 10$ ms (Fig. 1c) up to about 1 m/s at a time $t = 80$ ms (Fig. 1i).

The flow images in Figs. 1j and 1k (t =90 ms and $t = 100$ ms, respectively) show the second stage of the two-phase EHD flow development, i.e. initial stage of two-phase wall-impinging jet. In Fig. 1j (t = 90 ms) it can be seen that the EHD jet reached the plate electrode. Then at a time of $t = 100$ ms the jet impinged on the plate electrode surface (Fig. 1k). The velocity vector fields presented in Figs. 1j and 1k show that the flow velocity in the EHD jet core increased to about 1.5 m/s. However, the flow velocity of the EHD jet in the region of the impingement point (the flow stagnation area) was significantly lower, i.e. 0.3 m/s – 0.6 m/s.

Then the initial stage of two-phase wall-impinging jet evolved into the third stage of the EHD two-phase fluid flow, i.e. into the development stage of two-phase wall-impinging jet (Figs. 1 l–p, from $t = 110$ ms to $t = 383$ ms). After the jet has impinged the plate electrode two very regular vortices, rotating in the opposite directions were formed on both sides of the impingement point. In Fig. 1n (at a time $t = 183$ ms) it can be seen that the EHD two-phase fluid flow has already settled in the whole discharge chamber. The subsequent images in Figs. 1 n–p show that the vortices were moving along the plate electrode and finally left the camera observation area (Fig. 1q).

After a time of 650 ms (Fig. 1q) the vortices left the camera observation area and the fourth stage of the EHD two-phase fluid flow in the discharge chamber established, i.e. the fully developed two-phase EHD jet. At this stage the flow velocity in the EHD jet core was about 2.5 m/s. The further evolvement of the fully developed two-phase EHD jet was less spectacular in terms of the flow structure. However, due to continuous precipitation of the dust particles the two-phase flow has steadily been transforming into the single-phase flow, i.e. into the flow of the air void of the particulate matter.

Since the particle precipitation in the single needle-to-plate electrode arrangement closed in the relatively large chamber is a slow process, the transformation of the two-phase flow into the single-phase flow took some time.

Fig. 1r shows that the almost steady state single-phase EHD flow has been reached 30 s after the corona inception. In the fluid shown in Fig. 1r the concentration of air-suspended particles is very low (i.e. about 1000 particles/cm^3 compared with the initial concentration of about 450 000 particles/cm^3). This residual particulate matter had practically no influence on the EHD phenomena occurring at this stage of the flow evolvement. The remnants of smoke particles which have not been removed from the fluid could luckily be used as the fluid seeding necessary for the fluid imaging and the TR PIV measurements. Thus, it can be assumed that at this stage the EHD single-phase fluid flow was almost reached. As the velocity vector map shows (Fig. 1r) the EHD single-phase fluid flow (in the closed chamber) has the form of two large vortices with a relatively broad velocity core in the centre of interelectrode gap. The maximum velocity of the EHD single-phase fluid flow in the core axis was about 3 m/s.

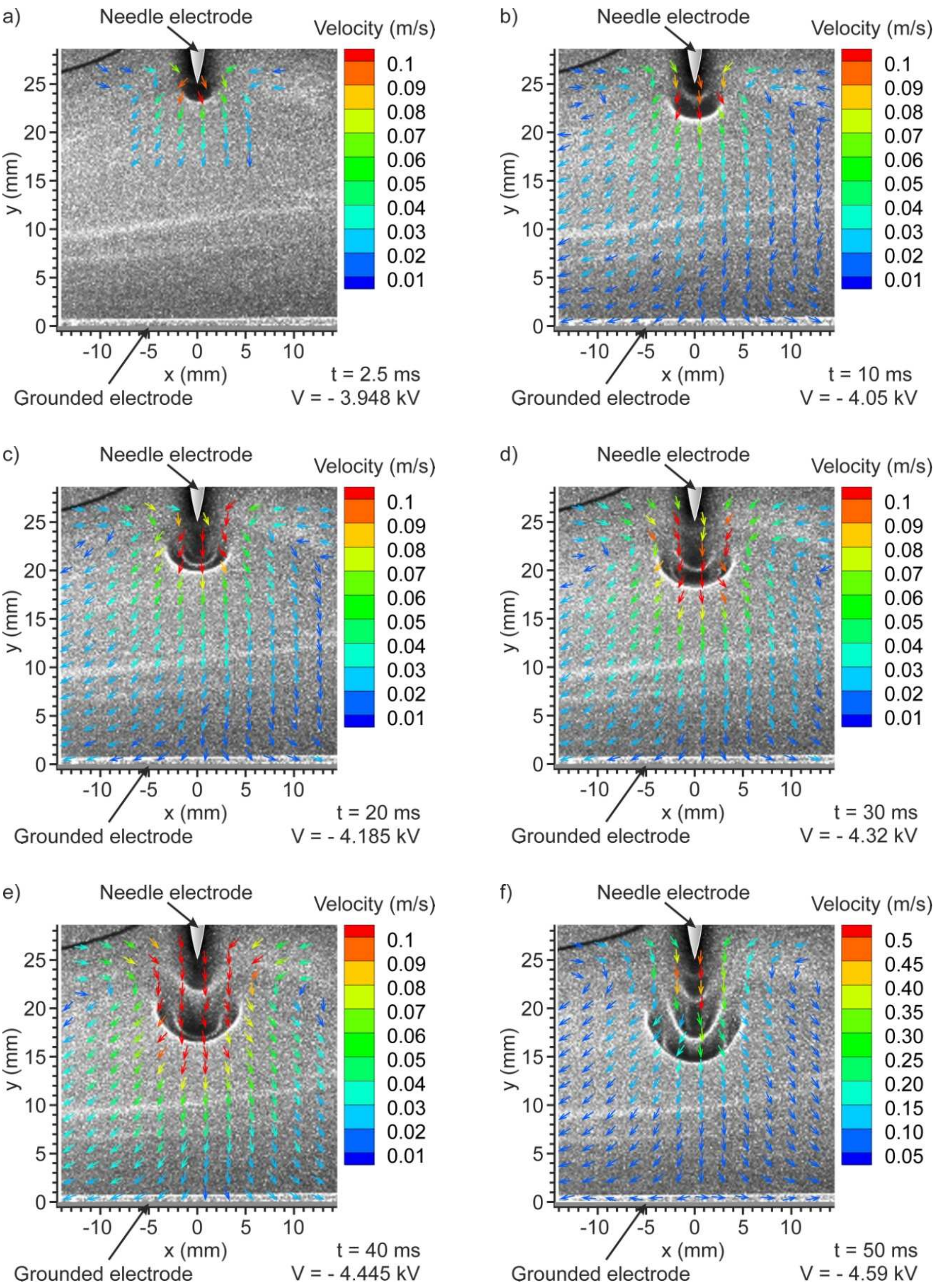

a)
Needle electrode
Velocity (m/s)
0.1
0.09
0.08
0.07
0.06
0.05
0.04
0.03
0.02
0.01
y (mm)
x (mm)
t = 2.5 ms
V = - 3.948 kV
Grounded electrode
b)
Needle electrode
Velocity (m/s)
t = 10 ms
V = - 4.05 kV
Grounded electrode
c)
Needle electrode
Velocity (m/s)
t = 20 ms
V = - 4.185 kV
Grounded electrode
d)
Needle electrode
Velocity (m/s)
t = 30 ms
V = - 4.32 kV
Grounded electrode
e)
Needle electrode
Velocity (m/s)
t = 40 ms
V = - 4.445 kV
Grounded electrode
f)
Needle electrode
Velocity (m/s)
0.5
0.45
0.40
0.35
0.30
0.25
0.20
0.15
0.10
0.05
t = 50 ms
V = - 4.59 kV
Grounded electrode

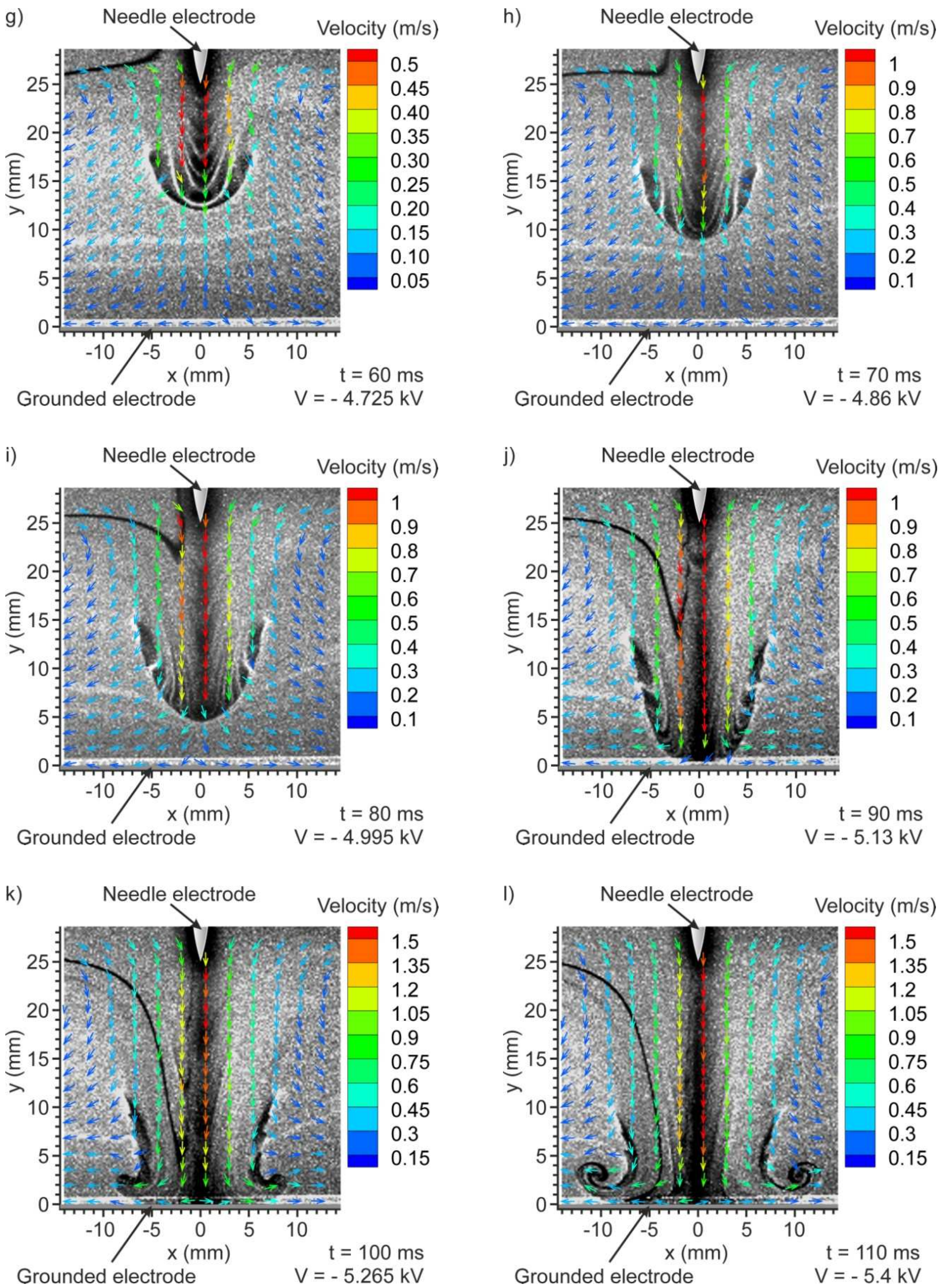
g)
Needle electrode
Velocity (m/s)
0.5
0.45
0.40
0.35
0.30
0.25
0.20
0.15
0.10
0.05
y (mm)
x (mm)
Grounded electrode
t = 60 ms
V = - 4.725 kV
h)
Needle electrode
Velocity (m/s)
1
0.9
0.8
0.7
0.6
0.5
0.4
0.3
0.2
0.1
Grounded electrode
t = 70 ms
V = - 4.86 kV
i)
Needle electrode
Grounded electrode
t = 80 ms
V = - 4.995 kV
j)
Needle electrode
Grounded electrode
t = 90 ms
V = - 5.13 kV
k)
Needle electrode
Velocity (m/s)
1.5
1.35
1.2
1.05
0.9
0.75
0.6
0.45
0.3
0.15
Grounded electrode
t = 100 ms
V = - 5.265 kV
l)
Needle electrode
Grounded electrode
t = 110 ms
V = - 5.4 kV

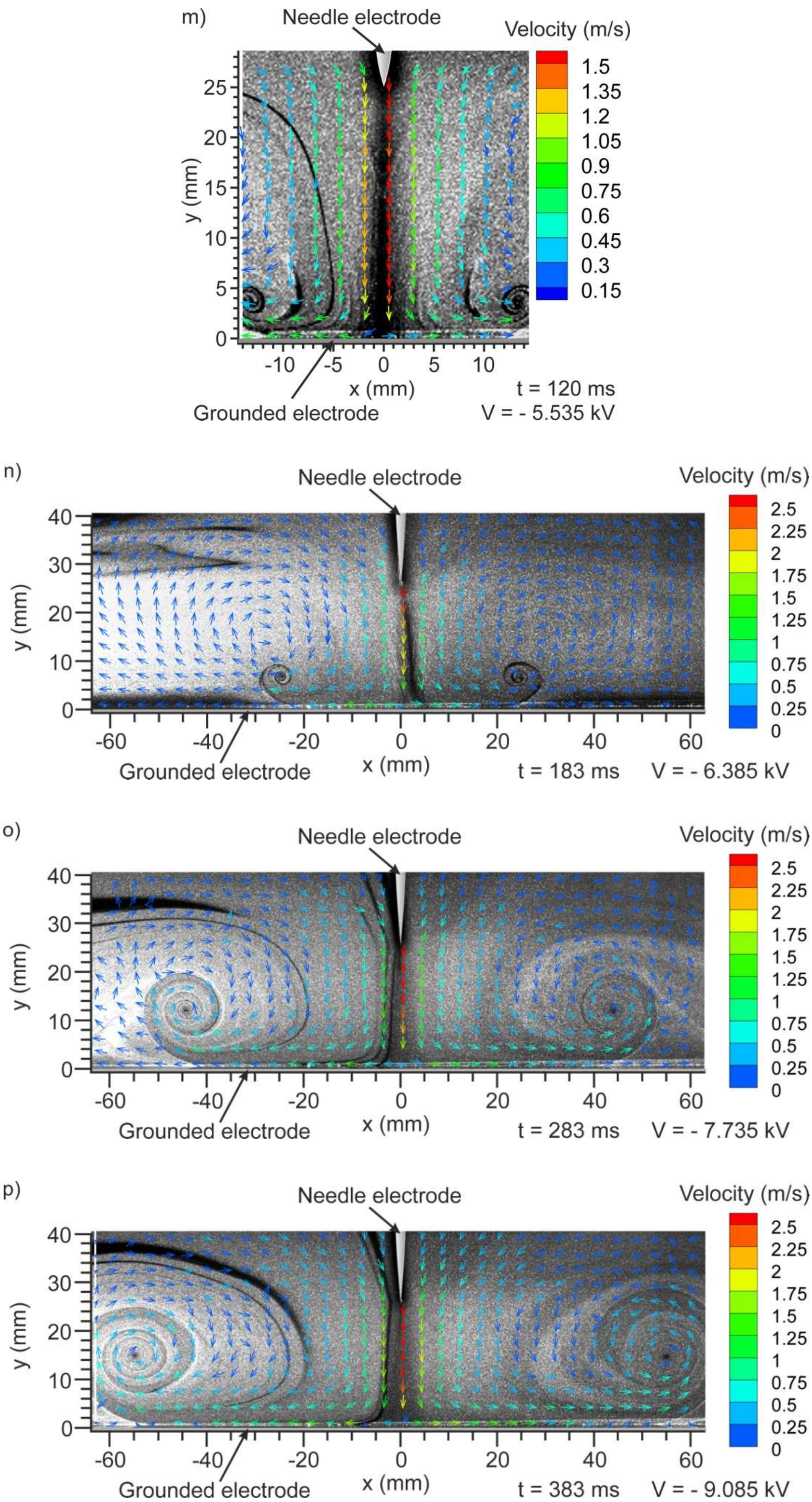
m)
Needle electrode
Velocity (m/s)
1.5
1.35
1.2
1.05
0.9
0.75
0.6
0.45
0.3
0.15
y (mm)
x (mm)
Grounded electrode
t = 120 ms
V = - 5.535 kV
n)
Needle electrode
Velocity (m/s)
2.5
2.25
2
1.75
1.5
1.25
1
0.75
0.5
0.25
0
y (mm)
x (mm)
Grounded electrode
t = 183 ms
V = - 6.385 kV
o)
Needle electrode
Velocity (m/s)
y (mm)
x (mm)
Grounded electrode
t = 283 ms
V = - 7.735 kV
p)
Needle electrode
Velocity (m/s)
y (mm)
x (mm)
Grounded electrode
t = 383 ms
V = - 9.085 kV

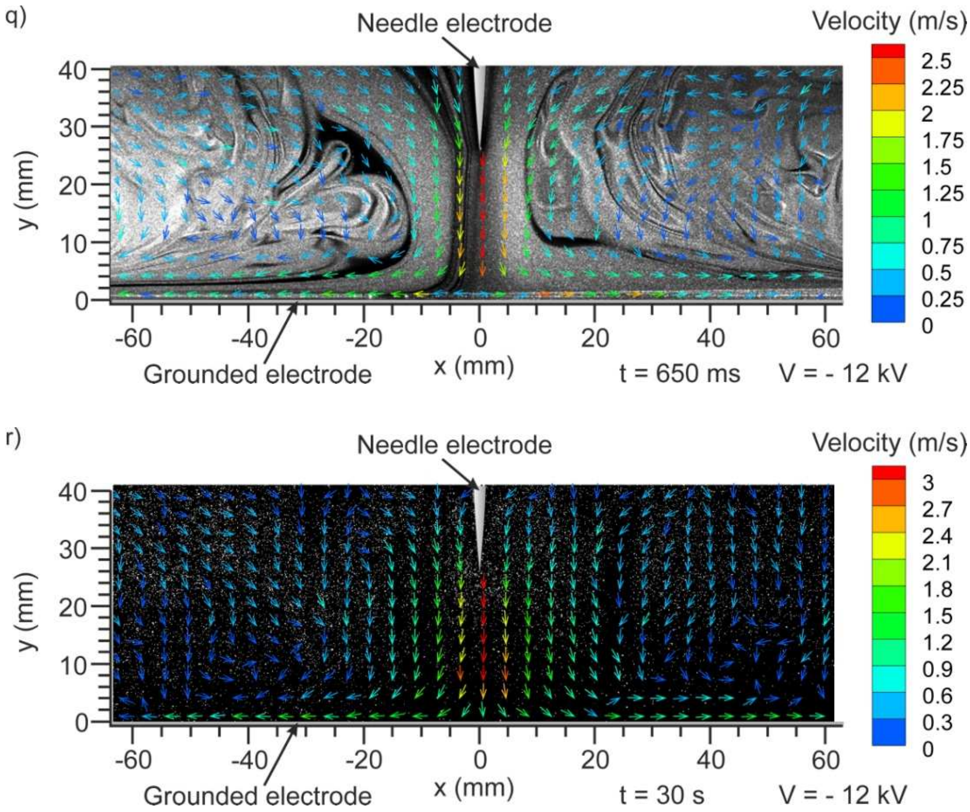

Figure 1. The flow images and the instantaneous velocity vector fields of the EHD two-phase fluid flow evolution in the needle-to-plate electrode arrangement after the negative corona inception for different times. The four transient stages of the EHD two-phase fluid flow development are shown: the two-phase free jet stage (from t = 2.5 ms to t = 80 ms), the initial stage of two-phase wall-impinging jet (from t = 90 ms to t = 100 ms, the development stage of two-phase wall-impinging jet (from t = 110 ms to t = 383 ms) and the fully developed two-phase EHD jet (at a time $\underline{t}$ = 650 ms). Also the almost single-phase steady-state flow structure is presented (at a time t = 30 s). The vectors show the smoke particle flow direction, the particle flow velocity magnitude can be read from the colour bar. The voltage rise rate 13.5 V/ms, the ultimate amplitude - 12 kV

4. Summary

The temporal and spatial evolution of the EHD two-phase fluid flow in the needle-to-plate electrode arrangement after the negative corona inception was investigated. The measurements were made in the initially motionless two-phase fluid (homogeneous mixture of air and incense smoke particles) closed in the discharge chamber. The results included instantaneous flow images and instantaneous velocity vector fields measured using TR PIV method.

The results showed that the evolvement of the initially motionless EHD two-phase fluid flow in the closed chamber can be divided into four transient structural flow stages, i.e. the two-phase free jet stage, the initial stage of two-phase wall-impinging jet, the development stage of two-phase wall-impinging jet and the fully developed two-phase EHD jet, and one final single-phase steady-state stage. This confirmed our prediction, given in the Introduction, that the two-phase EHD flow (air with homogeneously distributed particulate matter) should continuously evolve into the single-phase EHD flow (air void of the particulate matter).

Acknowledgments

The authors thank Mr Kacper Glowczewski for his technical assistance. This work was supported by the National Science Centre (grant UMO-2013/09/B/ST8/02054).

References

[1] Newton I., Optics, London, U.K., Printed for Sam. Smith, and Benj. Walford, Printers to the Royal Society, 1718.

[2] Leny R, Leny A.M., Boulloud A., in *Proc. 4th International Conference on Gas Discharges* Swansea, U.K., (1976), p. 246.

[3] Sigmond R.S., Electrical breakdown of gases. Meek J.M., Craggs J.D., 1978.

[4] Yabe A., Mori Y., Nijikate K, The American Institute of Aeronautics and Astronautics Journal 16, (1978), pp. 340–345.

[5] Crichton G.C., McAllister I.W., Brengsbo E., in *Proc. 14th International Conference on Phenomena in Ionized Gases*, Grenoble, France, (1979), pp. C7-287 - C7-288.

[6] Chang J.S., Journal of Aerosol Science, 12, (1981), pp. 19-26.

[7] Chang J.S., Lawless P.A., Yamamoto T., IEEE Transactions on Plasma Science, 19, (1991), pp. 1152-1166

[8] Chang J.S., Watson A., IEEE Transactions on Dielectics and Electrical Insulation, 1, (1994), pp. 871-895.

[9] Peterson R.J., Davidson J.H., in *Proc. IEEE Industry Applications Society Annual Meeting*, Denver, USA, (1994), pp. 1513-1518.

[10] Podlinski J., Niewulis A., Mizeraczyk J., Atten P., Journal of Electrostatics 66, (2008), pp. 246-253.

[11] Mizeraczyk J., Berendt A., Podlinski J., Niewulis A., International Journal of Plasma Environmental Science & Technology, 10, (2016), pp. 57-62.

[12] Mizeraczyk J., Berendt A., Podlinski J., Journal of Physics D: Applied Physics, 49, (2016), pp. 205203 (14 pages).

[13] See S.W., Balasubramanian R., Joshi U.M., Science and Technology of Advanced Materials, 8, (2007), pp. 25-32.